

Spin-dependent metastable He (2^3S) atom scattering from ferromagnetic surfaces: potential application to polarized gas production

Haruka Maruyama¹, Mitsunori Kurahashi^{2,*}, Kanta Asakawa¹, and Atsushi Hatakeyama^{1†}

¹Department of Applied Physics, Tokyo University of Agriculture and Technology, Koganei, Tokyo 184-8588, Japan

²National Institute for Materials Science, 1-2-1 Sengen, Tsukuba, Ibaraki 305-0047, Japan

(Dated: September 2, 2022)

A spin-polarized triplet metastable helium (He^*) beam has been used as a probe for surface magnetism, but changes in the spin state during scattering from a surface remain unclear. In the present study, we explored this issue by constructing an apparatus that allows us to direct a spin-polarized He^* beam to a surface and measure the spin polarization of He^* scattered from the surface. Magnetic hexapoles were used for both the beam polarization and the spin analysis. The results of the spin-dependent He^* scattering experiments on clean $\text{Fe}_3\text{O}_4(100)$, H-terminated $\text{Fe}_3\text{O}_4(100)$, benzene-adsorbed $\text{Fe}_3\text{O}_4(100)$, and non-magnetic $\text{Cu}(100)$ surfaces indicated that although the spin direction of He^* was mostly preserved during scattering from these surfaces, spin-flop scattering of survived He^* occurred with a probability up to approximately 0.1. Our results showed that the survival probability was higher when the spins of He^* and the $\text{Fe}_3\text{O}_4(100)$ film were parallel, which can be understood based on the lower He^* resonance ionization rate for this spin orientation. Based on our findings, we estimate that a non-polarized He^* gas becomes 10% spin-polarized after a single collision with a clean $\text{Fe}_3\text{O}_4(100)$ surface.

I. INTRODUCTION

Spin-polarized gaseous atoms have many research applications, including those involving atomic magnetometers [1], neutron spin filters [2], and magnetic resonance imaging of the lung [3]. Spin-polarized gases are often produced and used in containers, but spin depolarization due to collisions with container walls is detrimental to these applications. The effect of surface magnetism on depolarization, considered a key factor, has not yet been clarified due to a lack of experimental evidence.

In the field of condensed matter physics, the collision of spin-polarized particle beams with magnetic surfaces has been utilized to study surface magnetism. A spin polarized triplet metastable helium [$\text{He}^*(2^3S)$] beam, for which its magnetic sublevel is specified as $M_S = +1$ or -1 , has been used to investigate the spin polarization of the topmost surface of a solid [4]. Most He^* atoms de-excite on the vacuum side of the surfaces and induce the emission of surface electrons, for which the kinetic energy distribution is measured in spin-polarized metastable de-excitation spectroscopy (SPMDS) [4–8]. However, a fraction of impinging He^* survive the collision and are scattered from the surface. Previous studies have indicated that the survival probability ranges from 10^{-3} to 10^{-6} , depending on the surface electronic states [9–11] and the spin orientation of the incident He^* with respect to the surface spin[12]. However, it has remained unclear whether the spin state of He^* changes during scattering. Experimental verification is required, given the efficiency of spin depolarization in alkali atom scattering [13], as

well as phenomena that include the spin-flip scattering of polarized neutrons [14] and nuclear spin conversion of ortho- H_2 on surfaces [15]. Such information can also provide insight into the possibility of producing a spin-polarized gas via scattering from a ferromagnetic target.

In the present study, to determine how the spin state of He^* changes during scattering from a surface, we constructed an apparatus that allows us to direct a spin polarized triplet He^* beam to a surface and measure the spin polarization of scattered He^* . To reveal the effects of surface magnetism and surface termination, we conducted spin-dependent He^* scattering experiments with clean $\text{Fe}_3\text{O}_4(100)$, H-terminated $\text{Fe}_3\text{O}_4(100)$, benzene-adsorbed $\text{Fe}_3\text{O}_4(100)$, and non-magnetic $\text{Cu}(100)$ surfaces. The results indicated that although the He^* spin direction was mostly preserved during scattering, spin-flop scattering of survived He^* occurred with a probability up to approximately 0.1. We also found that the He^* survival probability was higher when spins of He^* and the $\text{Fe}_3\text{O}_4(100)$ film were parallel, which can be understood based on the lower He^* resonance ionization (RI) rate for this spin orientation. From these findings, we estimate that a non-polarized He^* gas becomes 10% spin-polarized after a single collision with a clean $\text{Fe}_3\text{O}_4(100)$ surface.

This paper is organized as follows. In Sec. II, we describe the experimental apparatus. The measurement of the spin polarization of survived He^* , together with the measurements of the survived He^* intensity and SPMDS spectra conducted for comparison, are presented in Sec. III. We discuss the spin flop of scattered He^* and possible polarization achieved by scattering of a non-polarized He^* beam on an $\text{Fe}_3\text{O}_4(100)$ surface in Sec. IV. The paper is concluded in Sec. V.

* KURAHASHI.Mitsunori@nims.go.jp

† hatakeya@cc.tuat.ac.jp

II. EXPERIMENTAL APPARATUS

A. Spin polarized He* beam

Figure 1 shows a schematic diagram of the experimental apparatus. All experiments were conducted in an ultrahigh vacuum chamber. The main part of the apparatus was the same as that used in our previous study [16]. A hexapole-type spin polarization analyzer for scattered He*, which will be described in Sec. II B, was added for the present study. He* atoms were generated by cold DC discharge and skimmed to produce the He* beam. He*(2^3S) atoms with a magnetic quantum number of $M_S = +1$ were focused with a hexapole magnet (the polarizer hexapole) [17] to pass through an aperture located downstream. He*(2^1S) and photons produced by discharge were removed by the center stop. The photons could not be completely blocked by the center stop and resulted in the background of the scattered He* signal. The background caused by scattering of the residual photons was not negligible, given that the He* survival probability was low. A leak valve attached to the hexapole chamber allowed us to introduce He gas to quench the He* atoms in the beam without changing the photon intensity. This enabled us to derive the photon background. M_S was defined with respect to the local magnetic field; its polarity could be flipped with a spin flipper that consisted of two longitudinal coils and a transverse coil. Stern-Gerlach analysis of the He* beam generated with a similar polarizer hexapole and a flipper [18] indicated that the $M_S = +1$ concentration in the non-flip mode was nearly 100%, whereas 90% of He* atoms were in the $M_S = -1$ state and 10% ($= \beta$) were in the $M_S = 0$ state in the flip mode. After the spin flipper, the He* spin state was adiabatically transported to the sample position, which was checked by analyzing the beam spin polarization using the method described in our previous paper [19]. The He* spin direction at the sample was controlled by applying a defining magnetic field (H) of 0.15 G using three-axis coils located behind the sample.

B. Spin polarization analysis of scattered He*

The spin polarization of the scattered He* atoms was analyzed with a combination of a hexapole, an aperture, and a channeltron, as illustrated in Fig. 1. The structure of this spin analyzer is the same as that used for the He* beam polarization analysis reported previously [19]. A hexapole with an identical structure to the polarizer hexapole was employed. This assembly was mounted on a tilt stage that allowed us to optimize the detection geometry. Because the analyzer hexapole focused (defocused) scattered He* atoms with $M_S = +1$ ($M_S = -1$), the He* atoms scattered to a larger steric angle were collected. This caused the detection efficiency for $M_S = +1$ to be much higher than for $M_S = -1$. Notably, the de-

tection efficiency for He* ($M_S = 0$), γ , was estimated to be 0.12[20]. In the present study, the He* beam impinged along the surface normal, and He* atoms scattered to 45° relative to the normal were detected.

The SPMDS measurement was performed by measuring the energy distribution of electrons ejected by He* using a hemispherical analyzer attached at 45° to the beam axis. The scattered He* and ejected electron intensities were measured at the same analysis point of the samples.

C. Spin configurations in the scattering

Four non-equivalent spin configurations exist, as shown in Fig. 2; these were realized by controlling the defining field direction at the sample and the spin flipper mode. For example, the non-flip (N) and parallel (P) mode [Fig. 2(a)] corresponds to the collision in which the He* spin direction remains unchanged when He* impinges on the surface with its spin parallel to the majority spin of the sample (S_M). This case is realized by setting the flipper to the N mode and directing H parallel to S_M . In the flip (F) and antiparallel (A) mode [Fig. 2(d)], the spin flipper is in the F mode and H is parallel to S_M .

D. Time-of-flight analysis

Measurement of the time-resolved intensities of scattered He* and ejected electrons while switching the flipper mode allowed us to conduct a time-of-flight (TOF) analysis of incident and scattered He*. Figure 3(a) shows the time-resolved intensities of He* scattered from a clean $\text{Fe}_3\text{O}_4(100)$ surface and accompanying ejected electrons. The spin configuration was changed from the N and P mode to the F and A mode at -5 ms, and then back to the N and P mode at 0 ms by switching the mode of the spin flipper. The intensities of scattered He* and ejected electrons then changed, due to the spin dependencies of the scattering and electron ejection processes, and the spin-dependent detection efficiency. The profile of the ejected electron (broken line) and scattered He*(solid line) [Fig. 3(a)] exhibits time delay from the switching signal. Here, we define t_1 as the TOF of the incident He* from the center of the spin flipper to the sample, and t_2 as the TOF of the scattered He* from the sample to the detector of the spin analyzer. The time delay of the ejected electron signal is nearly equal to t_1 because the electron's TOF is negligibly short. The time delay of scattered He* is equal to $t_1 + t_2$. Figure 3(b) shows the numerical derivatives of the time profiles in Fig. 3(a). The position of the peaks in Fig. 3(b) allows us to evaluate the kinetic energies of the incident and scattered He* atoms, which were 76 and 47 meV, respectively.

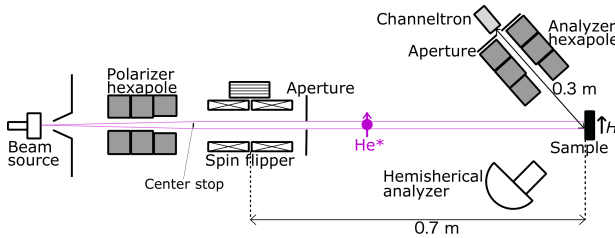


FIG. 1. Schematic diagram of the experimental apparatus. The distances from the center of the spin flipper to the sample, and from the sample to the entrance of the channeltron, were 0.7 and 0.3 m, respectively. The diameter of the apertures was 2 mm.

E. Sample preparation

$\text{MgO}(100)$ substrates were cleaned by degassing at 873 K under ultrahigh vacuum conditions and then annealing at 873 K for 15 min in an O_2 atmosphere. This annealing process completely removed carbon contamination, as verified by X-ray photoelectron spectroscopy. A 22-nm-thick Fe_3O_4 film was grown on the cleaned $\text{MgO}(100)$ substrate at 503 K by evaporating iron in an O_2 atmosphere with a deposition rate of 0.02 \AA/s for 180 min. Low-energy electron diffraction (LEED) clearly indicated $(\sqrt{2} \times \sqrt{2})R45^\circ$ reconstruction of the Fe_3O_4 surface, which agreed well with a previous report [21]. The Fe_3O_4 film was magnetized along the in-plane easy axis by applying a magnetic field generated by a coil near the sample. To prepare H-terminated $\text{Fe}_3\text{O}_4(100)$ surfaces, atomic H obtained by dissociating H molecules on a heated tungsten filament was adsorbed on clean $\text{Fe}_3\text{O}_4(100)$ films. The H-termination was confirmed by observing the LEED pattern reflecting the (1×1) structure [8, 22]. In the experiment on benzene-adsorbed surfaces, the H-terminated Fe_3O_4 substrate was cooled to 117 K before exposure to purified benzene vapor. A clean $\text{Cu}(100)$ surface was prepared by repeating 1 keV Ar^+ sputtering and annealing at 863 K.

III. RESULTS

Figure 4(a) shows the benzene exposure dependence of the intensity of He^* scattered from the H-terminated $\text{Fe}_3\text{O}_4(100)$ measured at the four spin configurations illustrated in Fig. 2. I_{NP} , I_{NA} , I_{FP} , and I_{FA} represent the intensities of scattered He^* in N and P mode, N and A mode, F and P mode, and F and A mode, respectively. The background due to the scattered photons described in Section II A was subtracted from the He^* intensity. The results show that intensity increases largely with benzene exposure at 0–10 L (1 L = $1.3 \times 10^{-4} \text{ Pa}\cdot\text{s}$). The difference in intensity between the P and A modes is also found in this exposure range. Figure 4(b) shows the ejected electron intensities in the P and A modes, which are represented as i_{P} and i_{A} , respectively, monitored at

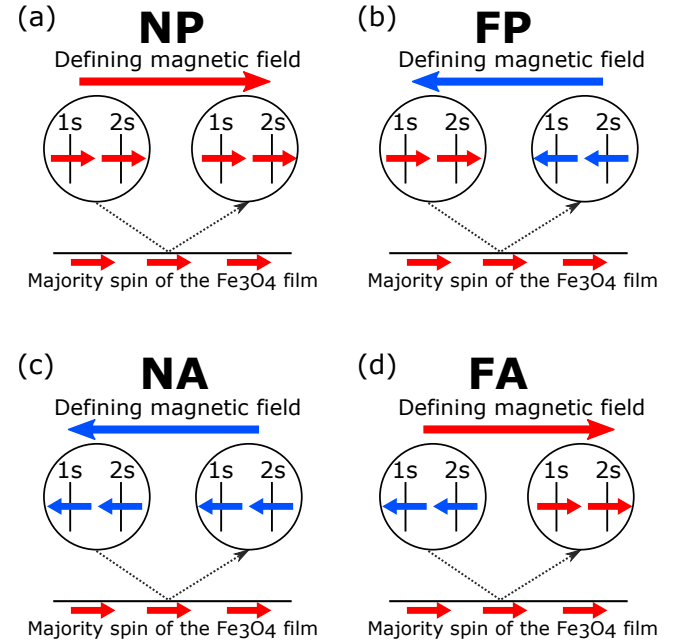


FIG. 2. Schematic illustration of the incident and measured spin states in the four spin modes. (a) Non-flip and parallel mode. (b) Flip and parallel mode. (c) Non-flip and antiparallel mode. (d) Flip and antiparallel mode.

an energy of 10 eV. The ejected electron intensities show clear dependencies on the benzene exposure and spin orientation at 0–10 L.

These behaviors are associated with the variation in benzene coverage and the He^* deexcitation mechanism on the surface. On the unexposed H-terminated $\text{Fe}_3\text{O}_4(100)$ surface, He^* decays via RI, followed by Auger neutralization (AN). The broad feature of the SPMDS spectra at 0 L shown in the inset of Fig. 4(b) confirms this. Benzene adsorbs molecularly on the surface. Its monolayer forms at approximately 5 L, a multilayer island begins to form at 5 L, and the whole surface is covered with a multilayer at approximately 10 L [22, 23]. The SPMDS spectra at 25 L [Fig. 4(b) inset] showing photoemission-like features reflect the multilayer formation, as well as He^* deexcitation via the Auger deexcitation (AD) process. Here, because the RI is more efficient than AD [24], the intensity of surviving He^* is higher at larger exposures [Fig. 4(a)]. The clean and submonolayer covered surfaces are spin polarized, causing the spin dependence in surviving He^* and the ejected electron intensities at 0–10 L.

Figure 4(c) shows the intensity ratio of the scattered He^* between spin configurations (F-N ratio). The F-N ratio roughly represents the spin-flopping probability, which will be discussed in more detail in Sec. IV A. There are two cases where the He^* spin direction changes; R_{P} (R_{A}), which is defined by the following formula, corresponds to the case in which the incident He^* spin is par-

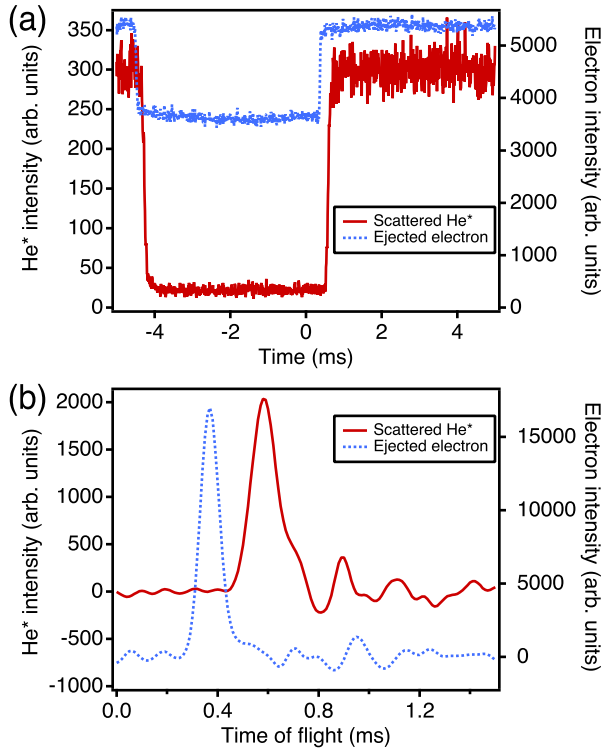


FIG. 3. (a) Time-resolved intensities of He^* scattered from a clean $\text{Fe}_3\text{O}_4(100)$ surface and accompanying ejected electrons. The spin configuration was changed at -5 ms and 0 ms by switching the mode of the spin flipper as described in the text. (b) Time-of-flight spectra derived by differentiating the profiles of (a).

allel (antiparallel) to S_M .

$$R_P = \frac{I_{\text{FP}}}{I_{\text{NP}}}, \quad (1)$$

$$R_A = \frac{I_{\text{FA}}}{I_{\text{NA}}}. \quad (2)$$

The very small values of these ratios indicate that the He^* spin direction is mostly preserved during scattering. However, these ratios also show clear exposure dependence [Fig. 4(c)], indicating that a transition between different magnetic sublevels of He^* happens during scattering from the surface. Small differences are discernible between R_P and R_A at low exposures; however, these differences have some uncertainty, based on the results for different runs that will be shown later [Fig. 5(b) inset].

As shown in Fig. 4(a), the intensity of scattered He^* exhibits a clear dependence on the spin orientation between incident He^* and S_M . To see these differences quantitatively, the spin asymmetries of scattered He^* intensities are defined as

$$A_{\text{He}^*} = \frac{I_{\text{NP}} - I_{\text{NA}}}{I_{\text{NP}} + I_{\text{NA}}}. \quad (3)$$

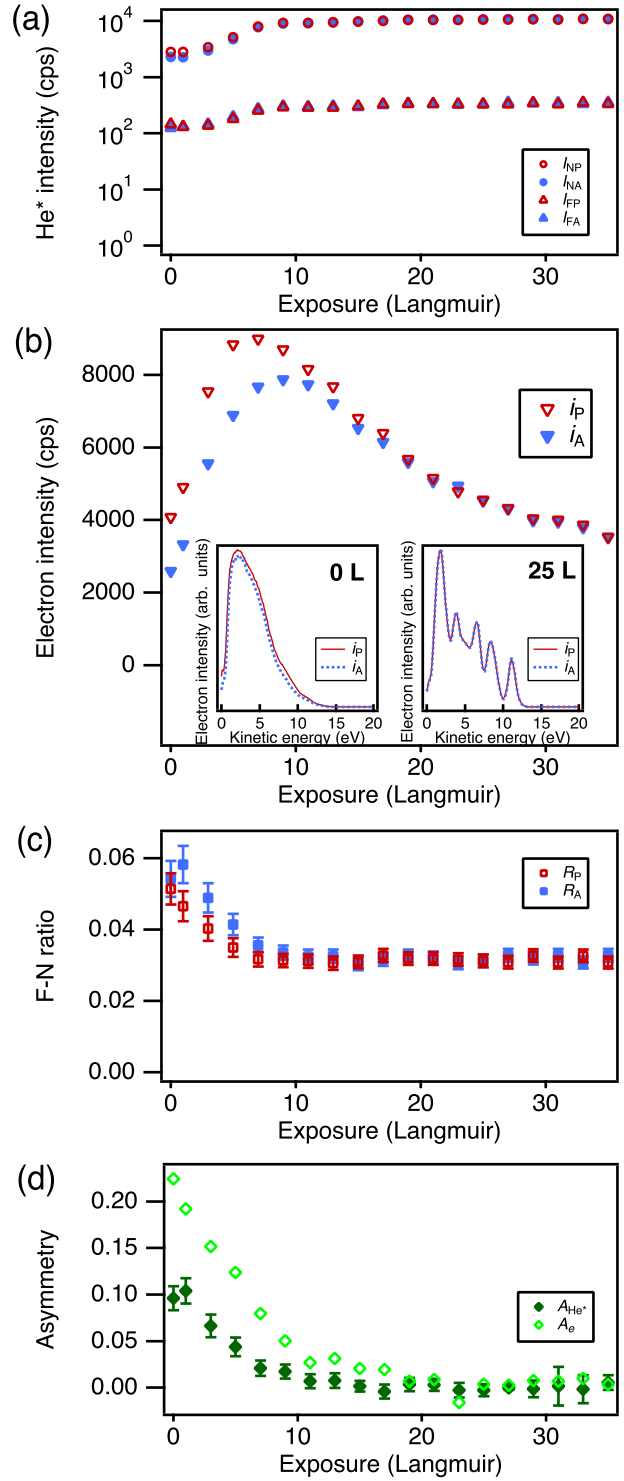


FIG. 4. (a) Benzene exposure dependence of scattered He^* intensities for the H-terminated $\text{Fe}_3\text{O}_4(100)$ surface, (b) the intensities of ejected electrons at 10 eV, (c) F-N ratios of scattered He^* intensities, and (d) spin asymmetries of scattered He^* and ejected electrons. Statistical errors are shown in (c) and (d). Insets in (b): SPMDS spectra

The spin asymmetry roughly represents the difference in spin-preserving survival probability between the P and A modes. They will be discussed in more detail in Sec. IV. Figure 4(d) shows the spin asymmetries of He^* and the electrons. The asymmetry in intensity of the ejected electrons at 10 eV A_e is defined as follows:

$$A_e = \frac{i_P - i_A}{i_P + i_A}. \quad (4)$$

A_{He^*} and A_e were 0.1 and 0.2 at 0 L, respectively. As the benzene exposure increased, A_{He^*} and A_e decreased and became zero at approximately 20 L. This exposure dependence is reasonable, given that the topmost surface of the multilayer benzene on H-terminated Fe_3O_4 is not spin-polarized.

Figure 5(a) shows a summary of the scattered He^* intensities in the four spin modes for clean $\text{Fe}_3\text{O}_4(100)$, H-terminated $\text{Fe}_3\text{O}_4(100)$, multilayered benzene on H-terminated $\text{Fe}_3\text{O}_4(100)$, and $\text{Cu}(100)$. Comparing intensities in the same spin modes, we found that those for clean and H-terminated $\text{Fe}_3\text{O}_4(100)$ were lower than those for benzene by factors of 4 and 3, respectively, whereas the intensity for Cu was lower by two orders of magnitude. These differences can be explained by the fact that He^* decays via the RI, followed by AN on clean and H-terminated $\text{Fe}_3\text{O}_4(100)$ and $\text{Cu}(100)$, whereas it decays via the AD process on the benzene multilayer [8, 10]; moreover, the survival probability is higher for oxidized metal surfaces than for non-oxidized metal surfaces [10].

Figure 5(b) summarizes the F-N ratios (R_P and R_A), which reflect the efficiency of the spin-flop scattering (as determined for the four surfaces). The inset shows the results for multiple experiments on H-terminated $\text{Fe}_3\text{O}_4(100)$, with error bars estimated assuming a Poisson distribution of the measured counts. The results show that (i) the F-N ratio for clean $\text{Fe}_3\text{O}_4(100)$ is higher than that for H-terminated $\text{Fe}_3\text{O}_4(100)$, although spin polarization at the Fermi level (E_F) is higher on the H-terminated surface [8]. (ii) A difference between R_P and R_A is discernible for the Fe_3O_4 surfaces, but is less clear when considering the results of multiple runs. (iii) The F-N ratio determined for a multilayer benzene-covered surface is clearly lower than that for other surfaces, and (iv) the F-N ratio for the magnetic Fe_3O_4 and non-magnetic $\text{Cu}(100)$ surfaces do not differ significantly.

Figure 5(c) summarizes the A_{He^*} values, which reflect the spin orientation dependence of the He^* survival probability. The results indicate that A_{He^*} for the clean Fe_3O_4 surface is higher than that for the H-terminated surface, although the spin polarization at E_F is lower on the clean $\text{Fe}_3\text{O}_4(100)$ surface. The much lower A_{He^*} on multilayer benzene reflects the fact that the topmost layer of multilayer benzene is nearly unpolarized.

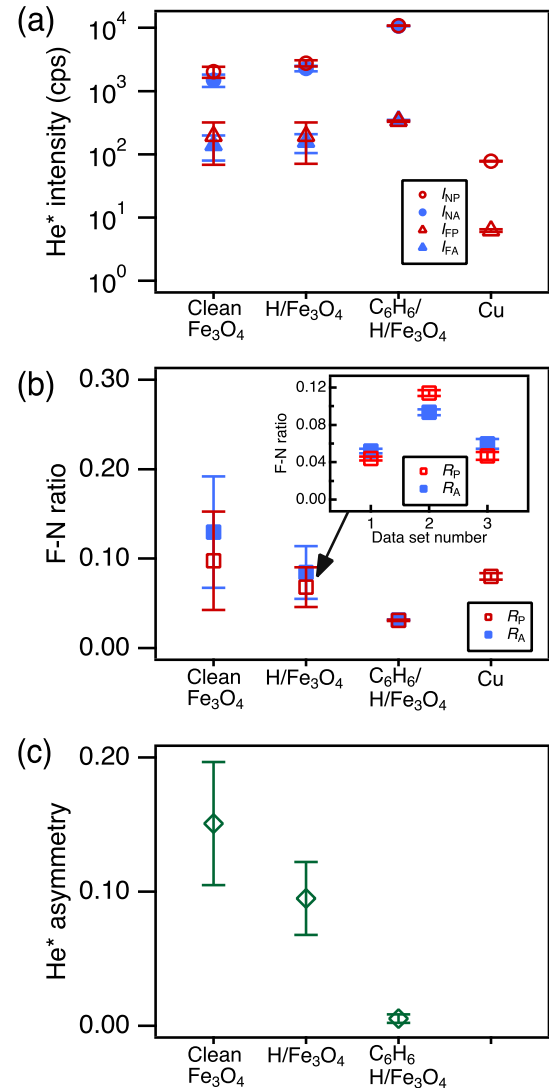


FIG. 5. (a) Scattered He^* intensities for clean $\text{Fe}_3\text{O}_4(100)$, H-terminated $\text{Fe}_3\text{O}_4(100)$, multilayered benzene on H-terminated $\text{Fe}_3\text{O}_4(100)$, and $\text{Cu}(100)$. (b) F-N ratios of intensities of scattered He^* . (c) Spin asymmetry of scattered He^* . For clean $\text{Fe}_3\text{O}_4(100)$ and H-terminated $\text{Fe}_3\text{O}_4(100)$, the means of multiple measurements are shown with standard deviations as error bars. Statistical errors are shown for the results of benzene and $\text{Cu}(100)$. Inset in (b): the F-N ratio of each measurement set for the H-terminated Fe_3O_4 surface.

IV. DISCUSSION

A. Spin flop scattering of He^*

First, we discuss the spin flop scattering of He^* . To characterize the dependence of the scattering processes on the spin directions, we consider the transition probability matrix (a_{ij}) and survival probability b_j . Incident He^* atoms with their spins parallel, antiparallel, and per-

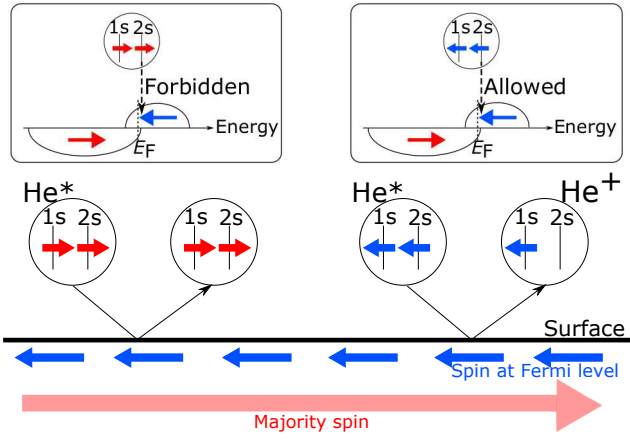


FIG. 6. Schematic illustration of the processes of He^* survival and deexcitation on the surface of $\text{Fe}_3\text{O}_4(100)$.

perpendicular to S_M , survive at probabilities of b_P , b_A , and b_0 , respectively. For surviving He^* atoms, the matrix element a_{ij} represents the transition probability from spin directions j to i , where $j = \text{P}$, A , and 0 represent the spin direction of the He^* atom parallel, antiparallel, and perpendicular to S_M before scattering, respectively, and $i = \text{P}$, A , and 0 represent the spin direction after scattering. If the scattering completely randomizes the spin states, all elements of the transition probability matrix are equal to $1/3$. If the scattering does not change the spin states at all, the diagonal elements of the transition probability matrix are equal to 1 , whereas the others are 0 . We assumed that our investigated scattering processes should be somewhere between these two extreme cases.

Using these transition probabilities, together with experimental parameters describing the efficiencies of the spin flipper and detector, $\beta = 0.10$ and $\gamma = 0.12$, respectively, I_{NP} , I_{NA} , I_{FP} , and I_{FA} can be expressed as follows:

$$I_{\text{NP}} = (a_{\text{PP}} + \gamma a_{0\text{P}})b_{\text{P}}I, \quad (5)$$

$$I_{\text{NA}} = (a_{\text{AA}} + \gamma a_{0\text{A}})b_{\text{A}}I, \quad (6)$$

$$I_{\text{FP}} = ((1-\beta)a_{\text{AP}}b_{\text{P}} + \beta a_{\text{A0}}b_0 + \gamma((1-\beta)a_{0\text{P}}b_{\text{P}} + \beta a_{00}b_0))I, \quad (7)$$

$$I_{\text{FA}} = ((1-\beta)a_{\text{PA}}b_{\text{A}} + \beta a_{\text{P0}}b_0 + \gamma((1-\beta)a_{0\text{A}}b_{\text{A}} + \beta a_{00}b_0))I. \quad (8)$$

Here, I is the incident He^* intensity. The meaning of the above expressions, for example, that of I_{FP} , is as follows. The He^* beam in the F mode contained $1 - \beta = 90\%$ He^* atoms in the $M_S = -1$ state and $\beta = 10\%$ in the $M_S = 0$ state. The impinging He^* atoms in the $M_S = -1$ and $M_S = 0$ states survived at probabilities of b_{P} and b_0 , respectively. We detected scattered He^* atoms that changed their magnetic substates from $M_S = -1$ to $M_S = +1$ at a probability of a_{AP} , from $M_S = 0$ to $M_S = +1$ at a probability of a_{A0} and from $M_S = -1$

to $M_S = 0$ at a probability of $a_{0\text{P}}$; they retained their magnetic substate in the $M_S = 0$ state at a probability of a_{00} . The detection efficiency of scattered He^* atoms in the $M_S = 0$ state was $\gamma = 0.12$, compared with the efficiency in the $M_S = +1$ state.

Using Eqs. (5), (6), (7) and (8), the F-N ratios are expressed as

$$R_{\text{P}} = \frac{I_{\text{FP}}}{I_{\text{NP}}} = \frac{a_{\text{AP}} + \beta(a_{\text{A0}}\frac{b_0}{b_{\text{P}}} - a_{\text{AP}}) + \gamma(a_{0\text{P}} + \beta(a_{00}\frac{b_0}{b_{\text{P}}} - a_{0\text{P}}))}{a_{\text{PP}} + \gamma a_{0\text{P}}} \quad (9)$$

$$R_{\text{A}} = \frac{I_{\text{FA}}}{I_{\text{NA}}} = \frac{a_{\text{PA}} + \beta(a_{\text{P0}}\frac{b_0}{b_{\text{A}}} - a_{\text{PA}}) + \gamma(a_{0\text{A}} + \beta(a_{00}\frac{b_0}{b_{\text{A}}} - a_{0\text{A}}))}{a_{\text{AA}} + \gamma a_{0\text{A}}} \quad (10)$$

For the benzene and Cu surfaces, which are not spin-polarized, the survival probabilities should be spin-independent. Thus, in the case of perfect spin-randomizing scattering,

$$R_{\text{P}} = R_{\text{A}} = 1, \quad (11)$$

and in the case of perfect spin-preserving scattering,

$$R_{\text{P}} = R_{\text{A}} = \gamma\beta = 0.012. \quad (12)$$

The experimental results showed that the F-N ratios were 0.03 and 0.08 for benzene and Cu, respectively, which are larger than 0.012 . This implies that spin flopping occurred (i.e., the off-diagonal elements of the transition matrix were non-zero). The F-N ratios were even larger for clean Fe_3O_4 and H-terminated Fe_3O_4 . If we assume perfect spin-preserving (no spin-flopping) scattering with spin-dependent survival probabilities, $R_{\text{P}} = \gamma\beta b_0/b_{\text{P}}$ and $R_{\text{A}} = \gamma\beta b_0/b_{\text{A}}$. However, it is unrealistic for b_0/b_{P} and b_0/b_{A} to be large, approximately 10 , to explain the observed F-N ratios of approximately 0.1 , because it has been shown that $b_{\text{A}}/b_{\text{P}}$ is close to 1 (e.g., 0.85 for Fe surfaces) [12]. Thus, the assumption of no spin-flopping scattering was incorrect; the spin-flopping scattering occurred for Fe_3O_4 and H-terminated Fe_3O_4 surfaces, as well as for benzene and Cu surfaces, and the larger F-N ratios can be attributed to the larger spin flopping rates.

The spin configuration dependence of the F-N ratio may be difficult to resolve based on the present results, as no clear difference was found in the F-N ratio between the P and A modes [Fig. 5 (b)].

B. Spin asymmetry of scattered He^*

Figure 5(c) shows that the intensity of He^* scattered from clean and H-terminated $\text{Fe}_3\text{O}_4(100)$ depends on the

spin configuration. This can be understood as follows. The spin asymmetry, which is defined as Eq. (3), can be approximated using Eqs. (5) and (6), as follows:

$$A_{\text{He}^*} \simeq \frac{a_{\text{PP}}b_{\text{P}} - a_{\text{AA}}b_{\text{A}}}{a_{\text{PP}}b_{\text{P}} + a_{\text{AA}}b_{\text{A}}}, \quad (13)$$

where we neglect the matrix elements multiplied by the small factor γ . Here, given that $a_{\text{PP}} \sim a_{\text{AA}}$, A_{He^*} is expressed as follows:

$$A_{\text{He}^*} \simeq \frac{b_{\text{P}} - b_{\text{A}}}{b_{\text{P}} + b_{\text{A}}}. \quad (14)$$

Figure 5(c) shows $A_{\text{He}^*} > 0$ for clean and H-terminated $\text{Fe}_3\text{O}_4(100)$, implying that the survival probability is higher when the He^* spin is parallel to S_M . Similar to the case of He^* scattering from Fe [12], this finding can be understood based on the spin dependence in the RI rate. Figure 6 illustrates the density of states (DOS) of the $\text{Fe}_3\text{O}_4(100)$ surface [8]. When He^* approaches the surface, its 2s state overlaps with a surface unoccupied state with the same spin, causing the RI. Because the spin-down DOS is higher than the spin-up DOS near E_F on $\text{Fe}_3\text{O}_4(100)$, the RI rate is higher and the survival probability is lower when the He^* spin is antiparallel to S_M . This explains the positive A_{He^*} .

Figure 5(c) shows that A_{He^*} is higher for clean $\text{Fe}_3\text{O}_4(100)$ than for the H-terminated surface. This finding can be understood by considering the contribution of He^* scattering from the surface oxygen atom. Although the Fe atom on H-terminated $\text{Fe}_3\text{O}_4(100)$ is highly spin-polarized at E_F , the spin polarization of the unoccupied local DOS at oxygen is higher on a clean Fe_3O_4 than on an H-terminated surface [8]. Additionally, the survival probability is higher when it is scattered by oxygen than by Fe on the topmost surface [10]. Thus, He^* atoms with spins parallel to the Fe_3O_4 spins near the Fermi level were filtered out to a greater extent by scattering on the Fe_3O_4 surfaces.

From the above experimental observation, we expect to obtain polarized He^* atoms when non-polarized He^* atoms are scattered on clean or H-terminated $\text{Fe}_3\text{O}_4(100)$. When the incident He^* beam is non-polarized, the polarization P of the scattered He^* is given by

$$P = \frac{\sum_j (a_{\text{P}j} - a_{\text{Aj}})b_j}{\sum_{ij} a_{ij}b_j}. \quad (15)$$

Considering that the off-diagonal elements of the transition probability matrix are sufficiently small compared to the diagonal elements a_{PP} , a_{00} and a_{AA} , we can estimate the polarization of scattered He^* as

$$P \simeq \frac{a_{\text{PP}}b_{\text{P}} - a_{\text{AA}}b_{\text{A}}}{\sum_j a_{jj}b_j}. \quad (16)$$

Assuming $a_{00}b_0$ is the mean of $a_{\text{PP}}b_{\text{P}}$ and $a_{\text{AA}}b_{\text{A}}$, we obtain

$$P \simeq \frac{2}{3}A_{\text{He}^*}. \quad (17)$$

The polarizations expected for scattered He^* in the case of non-polarized incident He^* are therefore 0.10 for clean $\text{Fe}_3\text{O}_4(100)$ and 0.06 for H-terminated $\text{Fe}_3\text{O}_4(100)$.

V. CONCLUSIONS

We constructed an apparatus comprising a spin-polarized He^* source and a hexapole-type spin analyzer for scattered He^* to evaluate the change in the spin state of He^* during scattering from a surface. The experiments on clean and H-adsorbed $\text{Fe}_3\text{O}_4(100)$ surfaces and a $\text{Cu}(100)$ surface indicated that although the magnetic sublevel of He^* is mostly preserved during the scattering, the transition between different sublevels happens with a probability of approximately 0.1 or less. We also observed the dependence of the He^* survival probability on the spin orientation of He^* and the Fe_3O_4 surface; this probability was associated with the spin-dependent RI rate. These findings imply that the spins of He^* atoms can be filtered by scattering on ferromagnetic surfaces.

The spin filtering described implies that He^* should become polarized when scattered on ferromagnetic surfaces. This could be exploited to generate polarized gases with spins on solid surfaces, such as ferromagnetic and spintronic materials. Additionally, more detailed studies to elucidate the transition mechanisms of the spin states may lead to a new method for surface magnetism characterization.

ACKNOWLEDGMENTS

This work was supported by the Sasakawa Scientific Research Grant from The Japan Science Society, National Institute for Materials Science (NIMS) Joint Research Hub Program, JSPS KAKENHI Grant Numbers 20H02623, 20K21148, and the Doctoral Program for World-leading Innovative & Smart Education (WISE program) of Tokyo University of Agriculture and Technology (TUAT) granted by the Ministry of Education, Culture, Sports, Science and Technology (MEXT), Japan.

-
- [1] H. B. Dang, A. C. Maloof, and M. V. Romalis, Ultrahigh sensitivity magnetic field and magnetization measurements with an atomic magnetometer, *Applied Physics Letters* **97**, 151110 (2010), <https://doi.org/10.1063/1.3491215>.
- [2] T. Okudaira, T. Oku, T. Ino, H. Hayashida, H. Kira, K. Sakai, K. Hiroi, S. Takahashi, K. Aizawa, H. Endo, S. Endo, M. Hino, K. Hirota, T. Honda, K. Ikeda, K. Kakurai, W. Kambara, M. Kitaguchi, T. Oda, H. Ohshita, T. Otomo, H. Shimizu, T. Shinohara, J. Suzuki, and T. Yamamoto, Development and application of a ${}^3\text{He}$ Neutron Spin Filter at J-PARC, *Nuclear Instruments and Methods in Physics Research Section A: Accelerators, Spectrometers, Detectors and Associated Equipment* **977**, 164301 (2020).
- [3] E. J. van Beek, J. M. Wild, H.-U. Kauczor, W. Schreiber, J. P. Mugler III, and E. E. de Lange, Functional MRI of the lung using hyperpolarized ${}^3\text{He}$ gas, *Journal of Magnetic Resonance Imaging* **20**, 540 (2004), <https://onlinelibrary.wiley.com/doi/pdf/10.1002/jmri.20154>.
- [4] M. Onellion, M. W. Hart, F. B. Dunning, and G. K. Walters, Spin-Polarized Metastable-Atom Deexcitation Spectroscopy: A New Probe of Surface Magnetism, *Phys. Rev. Lett.* **52**, 380 (1984).
- [5] M. S. Hammond, F. B. Dunning, G. K. Walters, and G. A. Prinz, Spin dependence in $\text{He}(2^3\text{S})$ metastable-atom deexcitation at magnetized $\text{Fe}(110)$ and $\text{O}/\text{Fe}(110)$ surfaces, *Phys. Rev. B* **45**, 3674 (1992).
- [6] M. Getzlaff, D. Egert, P. Rappolt, M. Wilhelm, H. Steidl, G. Baum, and W. Raith, Surface magnetic properties of oxygen on ferromagnetic films: a spin resolved MDS study, *Surface Science* **331-333**, 1404 (1995), proceedings of the 14th European Conference on Surface Science.
- [7] M. Salvietti, R. Moroni, P. Ferro, M. Canepa, and L. Mattera, Simple model to calculate surface magnetization from spin-polarized metastable deexcitation spectroscopy: $\text{Fe}/\text{Ag}(100)$, *Phys. Rev. B* **54**, 14758 (1996).
- [8] M. Kurahashi, X. Sun, and Y. Yamauchi, Recovery of the half-metallicity of an $\text{Fe}_3\text{O}_4(100)$ surface by atomic hydrogen adsorption, *Phys. Rev. B* **81**, 193402 (2010).
- [9] H. Conrad, G. Doyen, G. Ertl, J. Küppers, W. Sesselmann, and H. Haberland, Reflection of metastable he atoms from solid surfaces, *Chemical Physics Letters* **88**, 281 (1982).
- [10] H. Conrad, G. Ertl, J. Küppers, W. Sesselmann, B. Woratschek, and H. Haberland, Scattering of metastable rare gas atoms from solid surfaces, *Surface Science* **117**, 98 (1982).
- [11] P. Fouquet, P. Day, and G. Witte, Metastable (2^3S) helium atom scattering from $\text{NiO}(100)$ and $\text{Cu}(100)$ surfaces, *Surface Science* **400**, 140 (1998).
- [12] M. Kurahashi, T. Suzuki, X. Ju, and Y. Yamauchi, Spin dependence in the survival probability of metastable He (2^3S) atoms during the scattering from ferromagnetic surfaces, *Phys. Rev. Lett.* **91**, 267203 (2003).
- [13] N. Sekiguchi, A. Hatakeyama, K. Okuma, and H. Usui, Scattering of an alkali-metal atomic beam on anti-spin-relaxation coatings, *Phys. Rev. A* **98**, 042709 (2018).
- [14] R. M. Moon, T. Riste, and W. C. Koehler, Polarization Analysis of Thermal-Neutron Scattering, *Phys. Rev.* **181**, 920 (1969).
- [15] K. Fukutani and T. Sugimoto, Physisorption and ortho-para conversion of molecular hydrogen on solid surfaces, *Progress in Surface Science* **88**, 279 (2013).
- [16] M. Kurahashi and X. Sun, Observation of a half-metallic interface state for Pyridine-Adsorbed $\text{H}/\text{Fe}_3\text{O}_4(100)$, *The Journal of Physical Chemistry Letters* **12**, 8489 (2021).
- [17] G. Baum, W. Raith, and H. Steidl, Production of a spin-polarized, metastable $\text{He}(2^3\text{S})$ beam for studies in atomic and surface physics, *Zeitschrift für Physik D Atoms, Molecules and Clusters* **10**, 171 (1988).
- [18] M. Kurahashi, S. Entani, and Y. Yamauchi, Surface magnetization measurement with a spin-polarized metastable He beam under high magnetic fields of 0–5T, *Review of Scientific Instruments* **79**, 073902 (2008), <https://doi.org/10.1063/1.2949385>.
- [19] M. Kurahashi, Use of hexapole magnet and spin flipper combined with time-of-flight analysis to characterize state-selected paramagnetic atomic/molecular beams, *Review of Scientific Instruments* **92**, 013201 (2021), <https://doi.org/10.1063/5.0031903>.
- [20] We placed the same spin analyzer in the beamline and measured the change in the detector signal when changing the spin flipper mode. The signal intensity for the flip mode was 0.012 of that for the non-flip mode. Because 10% of He^* in the beam for the flip mode is in the $M_S = 0$ state and 90% is in the $M_S = -1$ state, and the detection efficiency for $M_S = -1$ is negligibly small, we can estimate the detection efficiency for $M_S = 0$, which was 0.12 of that for $M_S = +1$.
- [21] M. Fonin, R. Pentcheva, Y. S. Dedkov, M. Sperlich, D. V. Vyalikh, M. Scheffler, U. Rüdiger, and G. Güntherodt, Surface electronic structure of the $\text{Fe}_3\text{O}_4(100)$: Evidence of a half-metal to metal transition, *Phys. Rev. B* **72**, 104436 (2005).
- [22] A. Pratt, M. Kurahashi, X. Sun, and Y. Yamauchi, Adsorbate-induced spin-polarization enhancement of $\text{Fe}_3\text{O}_4(001)$, *Journal of Physics D: Applied Physics* **44**, 064010 (2011).
- [23] M. Kurahashi and Y. Yamauchi, Effects of adsorbate-induced states on the metastable He atom scattering from water- and benzene-adsorbed $\text{Cu}(100)$, *Surface Science* **590**, 21 (2005).
- [24] W. Sesselmann, B. Woratschek, G. Ertl, J. Küppers, and H. Haberland, Penning ionization electron spectroscopy of molecular adsorbates on Pd and Cu surfaces, *Surface Science* **146**, 17 (1984).